J. Fluid Mech. (1992), *vol.* 242, *pp.* 117–143
Printed in Great Britain

On the use of the method of matched asymptotic expansions in propeller aerodynamics and acoustics

By H. H. BROUWER
National Aerospace Laboratory NLR, 1006 BM Amsterdam, The Netherlands

(Received 29 October 1990 and in revised form 30 January 1992)

The applicability of the method of matched asymptotic expansions to both propeller aerodynamics and acoustics is investigated. The method is applied to a propeller with blades of high aspect ratio, in a uniform axial flow. The first two terms of the inner expansion and the first three terms of the outer expansion are considered. The matching yields an expression for the spanwise distribution of the downwash velocity. A numerical application shows that the first two terms of the inner solution do not yield an acceptable approximation for the downwash velocity. However, recasting the analytical expressions into an integral equation, similar to Prandtl's lifting line equation for wings, yields results for both aerodynamic and acoustic quantities, which agree well with experimental results. The method thus constitutes a practical analysis method for conventional propellers.

1. Introduction

The method of matched asymptotic expansions has been proven to be a powerful tool for the analysis of the flow about airfoils of high aspect ratio. The essential elements of the method were outlined by Van Dyke (1964, 1975), who applied it to an airfoil in a uniform, incompressible flow. Many extensions of this first application have since been worked out by other authors. An application which bears a close relationship to the present study is the one considered by Van Holten (1975, 1976), who applied the method to a helicopter rotor in forward flight.

In the present work we will consider a propeller, with blades of high aspect ratio, in an axial compressible flow. The expansion parameter is the reciprocal of the aspect ratio. In contrast to Van Holten, who used a somewhat different formulation in terms of a so-called common field, we will follow Van Dyke's asymptotic matching rule as closely as possible. Within the latter formalism the flow variables are systematically expanded in the small parameter. In this paper, the first two terms of the inner expansion and the first three terms of the outer expansion for both the velocity and pressure field are derived.

It will be shown, however, that if these expressions are applied to a typical propeller, the resulting (first-order) downwash velocity is too large, i.e. the induced angle of attack is of the same order as the geometrical (i.e. zeroth-order) angle of attack, instead of a small perturbation. As the propeller considered has an aspect ratio which is quite representative of conventional propellers, this means that the flow about such propellers cannot be approximated by the first few terms of an asymptotic expansion in the reciprocal aspect ratio.

It seems that one of the conditions required for the asymptotic matching principle to be valid is not satisfied, i.e. the expansion parameter is not small enough to allow

for the existence of a region where both the inner and the outer solution are valid. A general discussion on the necessary conditions for the method can be found in, for example, Crighton & Leppington (1973) and Van Dyke (1975).

Nevertheless, the method of matched asymptotic expansions leads to some useful analytical expressions for both the aerodynamics and acoustics of conventional propellers. The expression for the downwash velocity can be used in an integral equation, similar to Prandtl's equation for wings (c.g. Prandtl & Tietjens 1957, ch. VI). The solution of this equation appears to yield an accurate description of the propeller aerodynamics, although it is not a consistent asymptotic approximation in contrast to the solutions of the method of matched asymptotic expansions itself. With respect to the acoustics, the method leads to an expression for the acoustic pressure, which consists of lift, thickness and pitching moment components. Unlike many other methods for propeller aerodynamics, e.g. Goldstein (1929) and Reissner (1937), no explicit assumptions about the location of the trailing vortices have to be made.

In comparison to lifting surface theory, e.g. Hanson (1985), Sparenberg (1984) and Schulten (1984), the present theory has the advantage that it does not require a detailed geometry handling; it will be shown that, in principle, five numbers per blade section are sufficient for an accurate calculation. Furthermore, in lifting surface theories the induced velocity is not incorporated, i.e. the lift on a blade section is assumed to be perpendicular to the local undisturbed flow velocity. A lifting surface theory, however, has the advantage that it can be applied to propfans, i.e. propellers characterized by highly swept blades of low aspect ratio. These properties are the opposite of the properties required for the present method to be useful. In view of this restriction the applicability of the theory is hardly affected if the tip speed is assumed to be subsonic, which is the usual operating condition for conventional propellers.

A further simplification is achieved by the application of thin airfoil theory (Glauert 1959, p. 87), in combination with the Prandtl–Glauert transformation (Liepmann & Puckett 1947, p. 138) for the inner solution, although this is not a prerequisite for the method. This implies that we will incorporate only first-order perturbations with respect to the main flow. Although all quantities can be fully determined in principle without this approximation, the numerical application is in general not a simple task, whereas the use of a thin airfoil theory reduces the numerical work involved considerably. Furthermore, it has been shown by Hanson & Fink (1979), that for propellers operating under subsonic conditions, the nonlinear terms contribute very little to the sound field.

In §2 we give the mathematical description of the problem and an outline of the solution through matched asymptotic expansions. It is shown how by this method the full problem is separated into a so-called inner problem and an outer problem. In §3 we derive the first-order solution of the outer problem. It is shown that the inner expansion of the outer solution determines the boundary conditions at 'infinity' for the inner problem. The zeroth- and first-order solutions of the inner problem are studied in §4. Although the details of the inner flow field are left open, a description of its far-field approximation is given, which is sufficient for the matching to the outer solution. The results for the inner solution are used in §5 for the derivation of the second-order outer solution. It is also shown how the outer solution can be expressed as a sum of propeller harmonics.

In §6 a numerical application to a tested model propeller is considered. This shows that the first two terms of the inner solution yield an unrealistic result for the

circulation about the propeller blades. An explanation for this failure, as compared to the equivalent theory for stationary wings, is discussed in §7, where we also consider an alternative approach, which consists of transforming the asymptotic approximation into an integral equation. In §8 we compare both the aerodynamic and acoustic results of this modified method to the experimental data. The agreement turns out to be good for the performance data, and reasonable for the acoustic data.

2. Mathematical description of the problem

We consider a propeller with B blades of a high aspect ratio in a uniform axial flow, which is subsonic relative to the propeller. Furthermore we assume that the flow is inviscid and that the influence of the hub on the flow can be neglected. The high aspect ratio allows the introduction of a small parameter, which we take to be the ratio of the chord at 0.7 radius to the radius of the propeller:

$$\epsilon = c_{0.7}/R. \tag{2.1}$$

The precise value of this parameter is irrelevant, as, for the moment, it is only used as a bookkeeping parameter.

In what follows all quantities are made dimensionless with the density and speed of sound at infinity, and the propeller radius. We use a cylindrical coordinate system in which the propeller is at rest, i.e. the coordinate system rotates with angular velocity Ω with respect to an inertial reference frame, see figure 1. The line $x = 0$, $\theta = 0$ is chosen to coincide with the pitch-change axis of one of the blades, which axis is thus supposed to be perpendicular to the x-axis. In this coordinate system we have a stationary problem and the Euler equations read (e.g. Vavra 1960, ch. 7):

$$\nabla\cdot(\rho\boldsymbol{v}) = 0, \tag{2.2a}$$

$$\rho(\boldsymbol{v}\cdot\nabla)\,\boldsymbol{v}+\nabla p = -\rho[2\boldsymbol{\Omega}\times\boldsymbol{v}+\boldsymbol{\Omega}\times(\boldsymbol{\Omega}\times\boldsymbol{r})], \tag{2.2b}$$

where ρ is the density, $\boldsymbol{v}$ the flow velocity, and p the pressure. $\boldsymbol{\Omega}$ is the angular velocity vector, in this case equal to $\Omega\boldsymbol{i}_x$, where $\boldsymbol{i}_x$ is the unit vector in the x-direction.

At infinity we have

$$\boldsymbol{U} = M\boldsymbol{i}_x - \Omega r\boldsymbol{i}_\theta, \quad \rho_\infty = 1, \quad p_\infty = 1/\gamma, \tag{2.3}$$

where M is the axial main flow Mach number and γ is the specific heat ratio. Equations (2.3) determine the boundary conditions at infinity, while the boundary conditions at the blades are determined by the blade geometry and the Kutta condition. We will not consider a boundary condition at the hub, but simply assume that the blade (abruptly) ends at $r = r_h$. This assumption significantly simplifies the analytical calculations, while details of the flow at the hub region have little influence on either the performance or the noise levels of a propeller. The main cause for this is the low speed of the flow relative to the blade at the hub.

If we want to find a solution for the pressure (or velocity) field in terms of an expansion in powers of ϵ, there are two ways of doing so. First we consider the case that the distance from the propeller blades is of order unity, in which case an expansion can indeed be found. This expansion is called the outer expansion and denoted by a superscript o:

$$p^{\mathrm{o}}(r,\theta,x) = p_0^{\mathrm{o}}(r,\theta,x)+\epsilon p_1^{\mathrm{o}}(r,\theta,x)+\epsilon^2 p_2^{\mathrm{o}}(r,\theta,x)+\ldots. \tag{2.4}$$

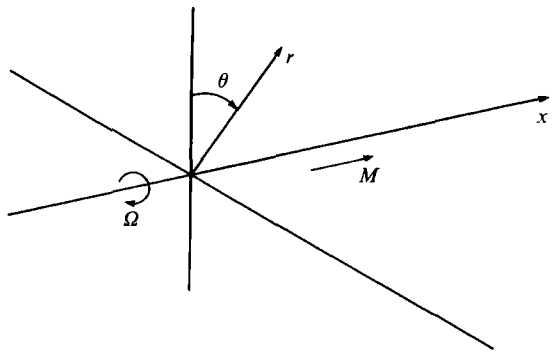

FIGURE 1. The cylindrical coordinate system.

This expansion, however, is not valid at field points in the vicinity of a blade. Furthermore, it contains some undetermined coefficients, as the boundary conditions at the blades cannot be imposed.

An expansion which is valid in the vicinity of a blade can be found by considering the distance to that blade to be of order ϵ. For field points near the blade at $\theta = 0$, for example, we thus define the so-called inner variables:

$$\bar{\theta} = \theta/\epsilon, \quad \bar{x} = x/\epsilon, \tag{2.5}$$

and write for the inner expansion:

$$p^{\mathrm{i}}(r, \bar{\theta}, \bar{x}) = p_0^{\mathrm{i}}(r, \bar{\theta}, \bar{x}) + \epsilon p_1^{\mathrm{i}}(r, \bar{\theta}, \bar{x}) + \epsilon^2 p_2^{\mathrm{i}}(r, \bar{\theta}, \bar{x}) + \ldots . \tag{2.6}$$

This expansion is neither fully determined nor is it valid at distances of the order of unity from the blade.

We now assume that a region exists where both expansions are valid, which can of course only be true if the inner and outer expansions can be related to each other. This should determine the coefficients that are still unknown. The most convenient way to establish the relation between the inner and outer expansions, is by use of the asymptotic matching principle (Van Dyke 1964, 1975). In each term of the outer expansion we replace x by $\epsilon\bar{x}$ and θ by $\epsilon\bar{\theta}$, and expand in ϵ. Anticipating the results of the next section we write

$$p_n^{\mathrm{o}}(r, \epsilon\bar{\theta}, \epsilon\bar{x}) = \epsilon^{-n}[p_{n0}^{\mathrm{o}} + \epsilon p_{n1}^{\mathrm{o}} + \epsilon^2 p_{n2}^{\mathrm{o}} + \ldots]. \tag{2.7}$$

In the same way we write

$$p_m^{\mathrm{i}}\left(r, \frac{\theta}{\epsilon}, \frac{x}{\epsilon}\right) = \epsilon^{-m}[p_{m0}^{\mathrm{i}} + \epsilon p_{m1}^{\mathrm{i}} + \epsilon^2 p_{m2}^{\mathrm{i}} + \ldots]. \tag{2.8}$$

The asymptotic matching principle is now stated as

$$\epsilon^m p_{nm}^{\mathrm{o}}(r, \bar{\theta}, \bar{x}) = \epsilon^n p_{mn}^{\mathrm{i}}(r, \theta, x). \tag{2.9}$$

Of course we could have written the same for the velocity or the density field. It should be noted that the expansions given above are incomplete, as usually not only powers of ϵ occur, but also powers of $\ln\epsilon$. According to Crighton & Leppington (1973), one should regard terms which are proportional to $\epsilon^n(\ln\epsilon)^1$ as being of order ϵ^n, which amounts to regarding $\ln\epsilon$ as being of order unity.

In this paper we will calculate p and v up to $n = 2$ and $m = 1$. In the next section we derive an expression for the outer expansion up to first order in ϵ.

3. The first-order outer solution

The Euler equations, as given by (2.2), are valid everywhere apart from the interior of the propeller blades. We can modify these equations to make them valid everywhere by introducing a function S, which is negative inside the blades, positive outside and zero on the surface of the blades. We then find from (2.2a):

$$\nabla\cdot H(S)\,[\boldsymbol{v}'+\boldsymbol{U}\rho'+\boldsymbol{v}'\rho'] = [\boldsymbol{v}'+\rho'\boldsymbol{v}]\cdot\nabla S\delta(S), \tag{3.1}$$

where $H(x)$ is the Heaviside step function, $\boldsymbol{v}' = \boldsymbol{v}-\boldsymbol{U}$ and $\rho' = \rho-1$.

As $\nabla S|_{S=0}$ is a vector along the normal on the surface, the second term in square brackets on the right-hand side of (3.1) makes no contribution. The remaining expression at the right-hand side is equal to $-\boldsymbol{U}\cdot\nabla S\,\delta(S)$. By using

$$(\boldsymbol{v}\cdot\nabla)\,\boldsymbol{U} = -\boldsymbol{\Omega}\times\boldsymbol{v} \tag{3.2}$$

and

$$\boldsymbol{\Omega}\times(\boldsymbol{\Omega}\times\boldsymbol{r}) = -\boldsymbol{\Omega}\times\boldsymbol{U} \tag{3.3}$$

we obtain from (2.2b)

$$\rho(\boldsymbol{v}\cdot\nabla)\,[H(S)\,\boldsymbol{v}']+\nabla[H(S)\,p'] = -\rho\boldsymbol{\Omega}\times H(S)\,\boldsymbol{v}'+[\rho\boldsymbol{v}'\boldsymbol{v}\cdot\nabla S+p'\nabla S]\,\delta(S), \tag{3.4}$$

where $p' = p-p_\infty$. Notice that again the first term in square brackets makes no contribution.

We now assume that we can write a multipole expansion for the remaining source terms, the first two terms of which are given by, respectively,

$$\boldsymbol{U}\cdot\nabla S\,\delta(S) \approx \frac{1}{r}\sum_{j=0}^{B-1}[Q_j(r)+\boldsymbol{P}_j(r)\cdot\nabla]\,\delta(x)\,\delta\left(\theta-\frac{2\pi j}{B}\right) \tag{3.5}$$

and

$$p'\nabla S\,\delta(S) \approx \frac{1}{r}\sum_{j=0}^{B-1}[-\boldsymbol{L}_j(r)+\boldsymbol{D}_j(r)\cdot\nabla]\,\delta(x)\,\delta\left(\theta-\frac{2\pi j}{B}\right), \tag{3.6}$$

where $\boldsymbol{D}_j$ is a tensor of rank two.

These equations imply that, in the derivation of the outer solution, the propeller is reduced to a system of rotating line singularities. This allows us to drop the Heaviside function in the rest of this section. We will now show that, at each order in ϵ, we have to incorporate only a limited number of singularities.

It is shown in Appendix A that $\boldsymbol{L}_j(r)$ is the lift per unit length on the blade section at r. Furthermore it can be shown that:

$$Q_j(r) = \int_{C_j(r)} \boldsymbol{U}\cdot\boldsymbol{n}\,\mathrm{d}l = 0, \tag{3.7}$$

$$\boldsymbol{P}_j(r) = \int_{C_j(r)} \boldsymbol{U}\cdot\boldsymbol{n}(\boldsymbol{r}-\boldsymbol{\rho})\,\mathrm{d}l \approx -A\,\boldsymbol{U}, \tag{3.8}$$

$$D_{j,xx}+D_{j,\theta\theta} = \int_{C_j(r)} p'(\boldsymbol{r}-\boldsymbol{\rho})\cdot\boldsymbol{n}\,\mathrm{d}l \approx 0, \tag{3.9}$$

$$D_{j,x\theta}-D_{j,\theta x} = -M_\mathrm{p}, \tag{3.10}$$

where $C_j(r)$ is the boundary contour of the section at r, A is the area enclosed by it, $\boldsymbol{\rho}$ is the dummy vector over which is integrated, $\mathrm{d}l$ is the differential arclength and $\boldsymbol{r}$ is the position vector of the intersection of the pitch change axis and the blade

section. M_p is the pitching moment. The last step in (3.8) and (3.9) is justified by the application of (first-order) thin airfoil theory, as already mentioned in the introduction.

As the lift scales on the chord, $\boldsymbol{L}_j$ is expanded as

$$\boldsymbol{L}_j(r) = \epsilon \boldsymbol{L}_{j,1}(r) + \epsilon^2 \boldsymbol{L}_{j,2}(r) + \dots . \tag{3.11}$$

The expansion for $\boldsymbol{D}_j$ starts with a term of order ϵ^2.

The lift is linear in the unit normal vector on the blade surface, $\boldsymbol{n}$, and as the r-component of $\boldsymbol{n}$ may be considered to be of order ϵ, we have

$$L_{j,1,r} \equiv 0. \tag{3.12}$$

The assumption that n_r is of order ϵ is of course not valid within a distance of order ϵ from the tip. A rigorous treatment of the tip would require the introduction of a third region in the calculation (besides the inner and outer regions), which should account for the influence of the radial flow and forces that are relatively important near the tip. In the present analysis they are of higher order and thus neglected. Their influence on the noise of a propfan is discussed by Hanson (1986). A discussion on the influence of the tip shape in the case of wing aerodynamics is given by Van Dyke (1964). Note that the r-components of $\boldsymbol{D}_{j,2}$ are also zero.

As the source terms are (at least) of first order in ϵ, the zeroth-order perturbations vanish, and we have, see (2.3),

$$\boldsymbol{v}_0^0 = \boldsymbol{U}, \quad \rho_0^0 = 1, \quad p_0^0 = 1/\gamma. \tag{3.13}$$

Note that we have assumed here that the derivatives in the Euler equations are of order unity or smaller. As the wavelength corresponding to the blade passing frequency is of the order of $2\pi/B\Omega$, and Ω is supposed to be smaller than unity, the assumption is valid for the first harmonics.

At first order we find for the (modified) Euler equations

$$\boldsymbol{\nabla} \cdot \boldsymbol{v}_1^0 + \boldsymbol{U} \cdot \boldsymbol{\nabla} \rho_1^0 = 0, \tag{3.14a}$$

$$(\boldsymbol{U} \cdot \boldsymbol{\nabla})\, \boldsymbol{v}_1^0 + \boldsymbol{\nabla} p_1^0 = -\boldsymbol{\Omega} \times \boldsymbol{v}_1^0 - \frac{1}{r} \sum_{j=0}^{B-1} \boldsymbol{L}_{j,1}\, \delta(x)\, \delta\left(\theta - \frac{2\pi j}{B}\right). \tag{3.14b}$$

This equation is similar to the equation considered by Wilmott (1988) in his treatment of the unsteady lifting-line problem for wings.

Using the isentropic relation between pressure and density, we have $\rho_1^0 = p_1^0$. Next we apply the operators $\boldsymbol{U} \cdot \boldsymbol{\nabla}$ and $\boldsymbol{\nabla} \cdot$ to (3.14a) and (3.14b) respectively, and subtract the results. We then obtain

$$[(\boldsymbol{U} \cdot \boldsymbol{\nabla})^2 - \boldsymbol{\nabla}^2] p_1^0 = \sum_{j=0}^{B-1} \boldsymbol{\nabla} \cdot \frac{1}{r} \boldsymbol{L}_{j,1}\, \delta(x)\, \delta\left(\theta - \frac{2\pi j}{B}\right), \tag{3.15}$$

where the differential operator at the right-hand side also applies to the δ-functions. We can obtain a Green's function for the operator at the left-hand side by transforming to the non-rotating frame of reference, which transforms this operator into that of a convective wave equation, for which the Green's function is well-known. Application to a rotating point source then gives the Green's function we are looking for:

$$G(r, \theta, x \,|\, \rho, \phi, \xi) = \frac{1}{4\pi\beta} \sum_k \frac{1}{|R_k - (\Omega r \rho/\beta) \sin(\psi_k)|}, \tag{3.16}$$

where we have to sum over the solutions of

$$R_k = \left[\left(\frac{x-\xi}{\beta}\right)^2 + r^2 + \rho^2 - 2r\rho\cos(\psi_k)\right]^{\frac{1}{2}}, \tag{3.17}$$

in which

$$\psi_k = \theta - \phi + \frac{\Omega}{\beta}\left[R_k - \frac{M}{\beta}(x-\xi)\right]; \tag{3.18}$$

β has the usual meaning of $(1-M^2)^{\frac{1}{2}}$.

It is not difficult to prove that, if $|r\rho\Omega|/\beta < 1$, there exists one and only one solution to (3.17). As long as we are only interested in matching the outer and inner solutions, we have $r < 1$, while $|\rho\Omega| < \beta$ is satisfied if the flow relative to the propeller at radius ρ is subsonic. Therefore, we drop the subscript k from here. One can also prove that, under the same conditions, $R - (\Omega r\rho/\beta)\sin\psi \geqslant 0$.

We now find for the solution of (3.15):

$$\begin{aligned} p_1^0 &= \sum_{j=0}^{B-1}\int_0^{2\pi}\int_{r_h}^1\int_{-\infty}^{\infty} \rho G(r,\theta,x\,|\,\rho,\phi,\xi)\,\nabla_s\cdot L_{j,1}\frac{1}{\rho}\delta(\xi)\,\delta\left(\phi-\frac{2\pi j}{B}\right)\mathrm{d}\xi\,\mathrm{d}\rho\,\mathrm{d}\phi \\ &= -\sum_{j=0}^{B-1}\int_{r_h}^1 \frac{1}{4\pi\beta R_{s,j}^3}\left\{rL_{j,1,\theta}\left[\sin(\psi_j) - \frac{\Omega}{\beta}R_j\cos(\psi_j)\right]\right. \\ &\quad \left. + \frac{1}{\beta^2}L_{j,1,x}\left[x\left(1-\frac{\Omega^2 r\rho}{\beta^2}\cos(\psi_j)\right) - r\rho\Omega M\left(\sin(\psi_j) - \frac{\Omega}{\beta}R_j\cos(\psi_j)\right)\right]\right\}\mathrm{d}\rho, \end{aligned} \tag{3.19}$$

where ∇_s is the gradient operator applied to the source coordinates (ρ, ϕ and ξ) and

$$\left.\begin{aligned} R_j &= \left[\left(\frac{x}{\beta}\right)^2 + r^2 + \rho^2 - 2r\rho\cos(\psi_j)\right]^{\frac{1}{2}}, \\ \psi_j &= \theta - \frac{2\pi j}{B} + \frac{\Omega}{\beta}\left[R_j - \frac{M}{\beta}x\right], \quad R_{s,j} = R_j - \frac{\Omega r\rho}{\beta}\sin(\psi_j). \end{aligned}\right\} \tag{3.20}$$

Note that the integration in the radial direction is limited by the hub radius, r_h, and the tip, $r = 1$, as there is no source outside this range.

Next we will calculate the first two terms of the inner expansion with respect to the blade at $\theta = 0$, i.e. with blade number $j = 0$. To do this we replace x by $\epsilon\bar{x}$ and θ by $\epsilon\bar{\theta}$ and expand in ϵ. In the terms with $j \neq 0$ one can take the limit $\epsilon \to 0$ without any problem, which means that these terms are of order ϵ^0. Once $L_{j,1}$ is known they can be calculated numerically, with x and θ set to zero.

For $j = 0$, however, the integrand, in the limit $\epsilon \to 0$, has a singularity at $\rho = r$, which cannot be integrated. This singularity occurs as the solution of (3.20) for $x = 0$, $\theta = 0$, and $\rho = r$ is given by $R_0 = 0$ and $\psi_0 = 0$. With $\rho = r + \zeta$ and $\zeta \lesssim \epsilon$, we have

$$R_0 = \frac{-\epsilon}{U\beta\beta_1^2}r\Omega(r\Omega\bar{s} + M\beta_1\bar{q}) + \frac{\beta^2}{\beta_1^2}R_{s,0} + O(\epsilon^2), \tag{3.21}$$

where $\beta_1 = [1 - M^2 - (\Omega r)^2]^{\frac{1}{2}}$

and

$$\psi_0 = \frac{-\epsilon}{rU\beta^2}(r\Omega\bar{s} + M\beta_1\bar{q}) + \frac{\Omega}{\beta}R_0 + O(\epsilon^2), \tag{3.22}$$

$$R_{s,0} = \frac{\epsilon}{\beta}\left[\bar{s}^2 + \bar{q}^2 + \left(\frac{\beta_1\zeta}{\epsilon}\right)^2\right]^{\frac{1}{2}} + O(\epsilon^2), \tag{3.23}$$

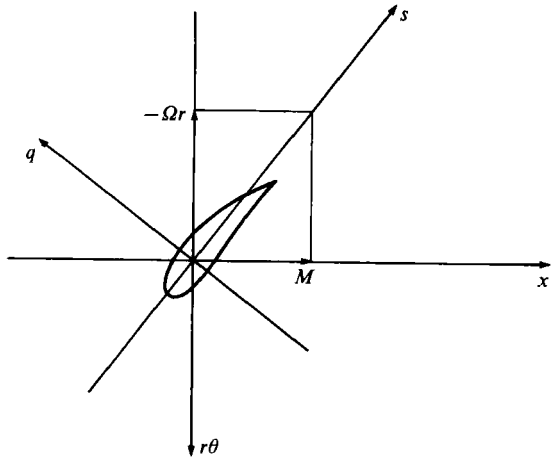

FIGURE 2. The local coordinates s and q.

where we have introduced the helicoidal coordinates s and q, and incorporated the local Prandtl–Glauert factor, see figure 2:

$$s = \frac{1}{U}(Mx - r\Omega r\theta), \quad q = -\frac{\beta_1}{U}(r\Omega x + Mr\theta). \tag{3.24}$$

The leading term of the inner expansion of p_1^0 is now given by

$$\frac{-1}{4\pi\beta^2}\{\bar{s}L_{0,1,s}(r) + \beta_1\bar{q}L_{0,1,q}(r)\}\int_{r_h-r}^{1-r}\left[\bar{s}^2+\bar{q}^2+\left(\frac{\beta_1\zeta}{\epsilon}\right)^2\right]^{-\frac{3}{2}}\mathrm{d}\zeta$$

$$\approx -\frac{1}{\epsilon}\frac{1}{4\pi\beta_1}\frac{\bar{s}L_{0,1,s}(r)+\beta_1\bar{q}L_{0,1,q}(r)}{\bar{s}^2+\bar{q}^2} \equiv \frac{1}{\epsilon}p_{10}^0, \tag{3.25}$$

where L_s and L_q are the components of $\boldsymbol{L}$ in the s- and q-directions, without incorporation of the Prandtl–Glauert factor, i.e. these components are obtained from L_x and L_θ by a rotation only. p_{10}^0 is the pressure field associated with the bound vortex along the blade. It can be shown that the remaining part of the term which is linear in $xL_{0,1,x}$ contains only terms of order ϵ and $\epsilon\ln\epsilon$, and is therefore a part of ϵp_{12}^0 (see the remark on the logarithmic terms in §2). We thus find

$$p_{11}^0 = \sum_{j=0}^{B-1}\int_{r_h}^{1}\frac{r}{4\pi U\beta^3}\left[\frac{1}{R_{s,j}^3}(\rho\Omega L_{j,1,s}+M\beta_1^2 L_{j,1,q})\left[\sin(\psi_j)-\frac{\Omega}{\beta}R_j\cos(\psi_j)\right]\right]_{s=0,q=0}\mathrm{d}\rho. \tag{3.26}$$

Next we turn to the calculation of the first-order velocity field, which we require to determine the downwash velocity at the blade. It can be obtained by integration of the first-order momentum equation, (3.14b), along the characteristics. The result is

$$\boldsymbol{v}_1^0 = -\frac{1}{M}\boldsymbol{\nabla}\int_0^\infty p_1^0\left(r,\theta+\frac{\Omega}{M}\xi, x-\xi\right)\mathrm{d}\xi - H(x)\frac{1}{r}\frac{U}{M}\sum_{j=0}^{B-1}L_{j,1}\,\delta\left(\frac{\Omega}{M}x+\theta-\frac{2\pi j}{B}\right). \tag{3.27}$$

Note that the path of integration in the first term coincides with the (zeroth-order) streamline through (r,θ,x). The second term is singular in the wake and zero

elsewhere. As this term plays no role in the matching process we will omit it in the rest of this section. It will be discussed further in §5.

The evaluation of the first two terms of the inner expansion of $\boldsymbol{v}_1^0$ is an important part of this paper. The θ-component is given by

$$v_{1,\theta}^0 = \frac{1}{4\pi\beta M}\sum_{j=0}^{B-1}\int_{r_h}^{1}\int_0^\infty \frac{1}{R_{s,j}^4}$$
$$\times\left\{L_{j,1,\theta}\left[\frac{-3r\rho}{R_{s,j}}\left(\sin(\psi_j)-\frac{\Omega}{\beta}R_j\cos(\psi_j)\right)^2+R_{s,j}\cos(\psi_j)+\frac{\Omega}{\beta}R_j^2\sin(\psi_j)\right]\right.$$
$$+\frac{1}{\beta^2}L_{j,1,x}\left[\frac{-3\rho}{R_{s,j}}\left(\sin(\psi_j)-\frac{\Omega}{\beta}R_j\cos(\psi_j)\right)\right.$$
$$\times\left[(x-\xi)\left(1-\frac{\Omega^2 r\rho}{\beta^2}\cos(\psi_j)\right)-r\rho\Omega M\left(\sin(\psi_j)-\frac{\Omega}{\beta}R_j\cos(\psi_j)\right)\right]$$
$$\left.\left.+(x-\xi)\frac{\Omega^2\rho}{\beta^2}R_j\sin(\psi_j)-\rho\Omega M\left(R_{s,j}\cos(\psi_j)+\frac{\Omega}{\beta}R_j^2\sin(\psi_j)\right)\right]\right\}\mathrm{d}\xi\,\mathrm{d}\rho, \quad (3.28)$$

where the coordinates are taken as in the integrand in (3.27). The integrand is singular at $\xi = 0$ for $j = 0$, $x = 0$, $\theta = 0$ and $\rho = r$. Let us write the term with $j = 0$ as

$$\int_{r_h}^{1} I(\rho)\,\mathrm{d}\rho. \quad (3.29)$$

As the main contributions to the ξ-integral, for $\rho \approx r$ and small values of x and θ, come from the region of small ξ, we can use the approximations given by (3.21)–(3.23), i.e.

$$R_0 \approx \frac{-1}{U\beta\beta_1^2}r\Omega\left(r\Omega s+M\beta_1 q-\frac{Ur\Omega}{M}\xi\right)+\frac{\beta^2}{\beta_1^2}R_{s,0}, \quad (3.30)$$

$$\psi_0 \approx \frac{-1}{rU\beta^2}\left(r\Omega s+M\beta_1 q-\frac{Ur\Omega}{M}\xi\right)+\frac{\Omega}{\beta}R_0, \quad (3.31)$$

$$R_{s,0} \approx \frac{1}{\beta}\left[\left(s-\frac{U}{M}\xi\right)^2+q^2+\beta_1^2(\rho-r)^2\right]^{\frac{1}{2}}. \quad (3.32)$$

Now we denote by $I_{as}(\rho)$ the approximation of $I(\rho)$ obtained by using (3.30)–(3.32), and

$$\sin(\psi_0) \approx \psi_0, \quad \cos(\psi_0) \approx 1, \quad \rho \approx r \quad (\text{except in } R_{s,0}), \quad (3.33)$$

and by keeping only the most divergent terms. This leads to

$$I_{as} = \frac{1}{4\pi\beta^3 UM}\int_0^\infty \frac{1}{R_{s,0}^3}\left\{\frac{3}{R_{s,0}^2\beta^2}\left[r\Omega s+M\beta_1 q-\frac{r\Omega U}{M}\xi\right]\right.$$
$$\left.\times\left[\left(s-\frac{U}{M}\xi\right)L_{0,1,s}(r)+\beta_1 qL_{0,1,q}(r)\right]-\left[r\Omega L_{0,1,s}+M\beta_1^2 L_{0,1,q}(r)\right]\right\}\mathrm{d}s, \quad (3.34)$$

where (3.32) for $R_{s,0}$ has to be used. Next we rewrite (3.29) as

$$\int_{r_h}^{1} I(\rho)\,\mathrm{d}\rho = \int_{r_h}^{1}[I(\rho)-I_{as}(\rho)]\,\mathrm{d}\rho+\int_{r_h}^{1} I_{as}(\rho)\,\mathrm{d}\rho. \quad (3.35)$$

The evaluation of the last integral is a bit laborious but straightforward. The result, expressed in inner coordinates, is

$$\int_{r_h}^{1} I_{as}(\rho)\,\mathrm{d}\rho = -\frac{1}{\epsilon}\frac{1}{2\pi\beta_1^2 U^2}\frac{(r\Omega\bar{s}+M\beta_1\bar{q})L_{0,1,s}+(-M\beta_1\bar{s}+r\Omega\bar{q})\beta_1 L_{0,1,q}}{\bar{s}^2+\bar{q}^2} + \frac{M}{4\pi U^2}L_{0,1,q}\frac{1-r_h}{(r-r_h)(1-r)}+O(\epsilon). \quad (3.36)$$

In the first term on the right-hand side of (3.35) the limit $\epsilon \to 0$ can be taken and we find

$$[v^0_{1,\theta}]_{j=0} = \frac{1}{\epsilon}v^0_{10,\theta}+\mathrm{P}\int_{r_h}^{1}[I(\rho)-I_{as}(\rho)]_{s=0,q=0}\,\mathrm{d}\rho+\frac{M}{4\pi U^2}L_{0,1,q}(r)\frac{1-r_h}{(r-r_h)(1-r)}, \quad (3.37)$$

where the first term is defined by the first term of the right-hand side of (3.36) and $\mathrm{P}\int$ denotes the Cauchy principal value. Furthermore we have

$$I_{as}(\rho)|_{s=0,q=0} = \frac{-M}{4\pi U^2}L_{0,1,q}(r)\frac{1}{(\rho-r)^2}. \quad (3.38)$$

This completes our considerations for $v^0_{1,\theta}$. For $v^0_{1,x}$ we have from (3.27):

$$v^0_{1,x} = \frac{r\Omega}{M}v^0_{1,\theta}-\frac{1}{M}p^0_1. \quad (3.39)$$

This yields for the lowest-order terms in the s- and q-directions:

$$\left.\begin{aligned} v^0_{10,s} &= \frac{1}{2\pi\beta_1 U}\frac{\bar{s}L_{0,1,s}(r)+\beta_1\bar{q}L_{0,1,q}(r)}{\bar{s}^2+\bar{q}^2}, \\ v^0_{10,q} &= \frac{1}{2\pi U}\frac{\bar{q}L_{0,1,s}(r)-\beta_1\bar{s}L_{0,1,q}(r)}{\bar{s}^2+\bar{q}^2}; \end{aligned}\right\} \quad (3.40)$$

$\boldsymbol{v}^0_{10}$ is the velocity field associated with the bound vortex along the blade, while $\boldsymbol{v}^0_{11}$ (the remaining part of the right-hand side of (3.37)) is the downwash velocity at the blade, as will be shown in the next section. If $\Omega = 0$ we have

$$\left.\begin{aligned} [v^0_{11,q}]_{j=0} &= \frac{1}{4\pi M}\left\{\mathrm{P}\int_{r_h}^{1}\frac{1}{(\rho-r)^2}[L_{0,1,q}(\rho)-L_{0,1,q}(r)]\,\mathrm{d}\rho \right.\\ &\left. -L_{0,1,q}(r)\frac{1-r_h}{(r-r_h)(1-r)}\right\} = \frac{1}{4\pi M}\mathrm{P}\int_{r_h}^{1}\frac{\mathrm{d}L_{0,1,q}(\rho)}{\mathrm{d}\rho}\frac{1}{\rho-r}\,\mathrm{d}\rho, \\ [v^0_{11,s}]_{j=0} &= 0, \end{aligned}\right\} \quad (3.41)$$

where we have assumed that $L_{0,1,q}(1) = L_{0,1,q}(r_h) = 0$. This result is familiar from wing theory. It can be shown that the expansion of $v^0_{1,r}$ starts with a term of order ϵ^0, but we will not consider this component any further.

4. The zeroth- and first-order inner solutions

We substitute $x = \epsilon\bar{x}$ and $\theta = \epsilon\bar{\theta}$ in (2.2) and expand in ϵ. At lowest order we find for the r-component of the momentum equation:

$$\rho^i_0(\boldsymbol{v}^i_0\cdot\boldsymbol{\nabla}_2)v^i_{0,r} = 0, \quad (4.1)$$

where $$\nabla_2 = i_x \frac{\partial}{\partial \bar{x}} + i_\theta \frac{1}{r} \frac{\partial}{\partial \bar{\theta}}.$$

A solution for $v^i_{0,r}$ which matches the outer solution, as far as the latter is known from §3, is

$$v^i_{0,r} \equiv 0. \tag{4.2}$$

This leaves us with a two-dimensional zeroth-order problem:

$$\nabla_2 \cdot (\rho^i_0 \boldsymbol{v}^i_0) = 0, \tag{4.3a}$$

$$\rho^i_0 (\boldsymbol{v}^i_0 \cdot \nabla_2) \boldsymbol{v}^i_0 + \nabla_2 p^i_0 = 0. \tag{4.3b}$$

An explicit solution to these equations depends on the geometry of the blade section at r, and on the matching to the outer solution. From the matching principle, (2.9) and (3.13), we immediately find

$$\boldsymbol{v}^i_{00} = \boldsymbol{U}, \quad \rho^i_{00} = 1, \quad p^i_{00} = 1/\gamma. \tag{4.4}$$

This means that the zeroth-order inner problem is the two-dimensional problem of a blade section in a uniform compressible flow with velocity $\boldsymbol{U}$. In principle, it does not matter which method is used to solve this problem; even experimental data can be used. For convenience we use the thin airfoil approximation in this paper. Within this approximation, the first-order lift on a section of the blade at $\theta = 0$ is thus given by

$$L_{0,1,q} = \tfrac{1}{2} U^2 \frac{c}{\epsilon} \frac{2\pi}{\beta_1} \operatorname{sgn}(\Omega)(\alpha - \alpha_0), \quad L_{0,1,s} = 0, \tag{4.5}$$

where c is the chord, α is the angle between $\boldsymbol{U}$ and the chord, and α_0 the angle of zero lift. The latter can be calculated from the camber line.

The equations for the next term in the outer expansions read

$$\nabla_2 \cdot \boldsymbol{v}^i_{01} + \boldsymbol{U} \cdot \nabla_2 p^i_{01} = 0, \quad (\boldsymbol{U} \cdot \nabla_2) \boldsymbol{v}^i_{01} + \nabla_2 p^i_{01} = 0. \tag{4.6a, b}$$

If we take the inner product of $\boldsymbol{U}$ with (4.6b) and subtract the result from (4.6a), we find:

$$[\nabla_2^2 - (\boldsymbol{U} \cdot \nabla_2)^2] \phi^i_{01} = 0, \tag{4.7}$$

where $\boldsymbol{v}^i_{01} = \nabla_2 \phi^i_{01}$. So the velocity potential satisfies the Laplace equation in the (s, q) coordinate frame. This means that we can make use of the fundamental solutions of the Laplace equation in two dimensions. It is obvious from the conservation of mass flow, the matching principle and (3.40), that only the vortex solution for the potential is required. We thus have

$$\phi^i_{01} = \Gamma_1 \chi / (2\pi) \tag{4.8}$$

where $\chi = \tan^{-1}(q/s)$, and Γ_1 is the first-order circulation. This yields

$$v^i_{01,s} = \frac{-1}{2\pi} \frac{q\Gamma_1}{s^2 + q^2}, \quad v^i_{01,q} = \frac{1}{2\pi} \frac{\beta_1 s \Gamma_1}{s^2 + q^2}. \tag{4.9}$$

The matching with (3.40) yields Kutta–Joukowski's theorem:

$$\Gamma_1 = -\frac{1}{U} L_{0,1,q} = -U \frac{c}{\epsilon} \frac{\pi}{\beta_1} \operatorname{sgn}(\Omega)(\alpha - \alpha_0). \tag{4.10}$$

The same results could have been obtained by matching the pressure field. We thus find that $\boldsymbol{v}^i_{01}$ (or $\boldsymbol{v}^o_{10}$) is the velocity field of the so-called bound vortex.

Next we consider (4.3) at second order:

$$\nabla_2 \cdot \boldsymbol{v}^i_{02} + \boldsymbol{U} \cdot \nabla_2 \rho^i_{02} = -\nabla_2 \cdot (p^i_{01} \boldsymbol{v}^i_{01}) + (\gamma - 1) p^i_{01} \boldsymbol{U} \cdot \nabla_2 p^i_{01}, \tag{4.11a}$$

$$(\boldsymbol{U} \cdot \nabla_2) \boldsymbol{v}^i_{02} + \nabla_2 \rho^i_{02} = -p^i_{01} (\boldsymbol{U} \cdot \nabla_2) \boldsymbol{v}^i_{01} - (\boldsymbol{v}^i_{01} \cdot \nabla_2) \boldsymbol{v}^i_{01}, \tag{4.11b}$$

where the isentropic relation between pressure and density has been used. The application of thin airfoil theory implies the neglecting of terms which are quadratic in the perturbation quantities, so the right-hand sides of (4.11*a*, *b*) are put to zero. Thus we also find for the second-order velocity potential:

$$[\nabla_2^2-(\boldsymbol{U}\cdot\nabla_2)^2]\,\phi_{02}^{\mathrm{i}}=0. \tag{4.12}$$

As $\boldsymbol{v}_{02}^{\mathrm{i}}$ is the second-order term in the outer expansion, its potential should be of first order in $(s^2+q^2)^{-\frac{1}{2}}$, which corresponds to a dipole source:

$$\phi_{02}^{\mathrm{i}}=-(s^2+q^2)^{-\frac{1}{2}}\frac{1}{2\pi}(N_{2,s}\cos\chi+N_{2,q}\sin\chi), \tag{4.13}$$

where $\boldsymbol{N}_2$ is the (second-order) dipole vector. In Appendix B it is shown how the components of a dipole source can be related to the area of the blade section and the pitching moment. This completes our considerations on the zeroth-order inner solution.

The equations for the first-order terms in the inner expansions are

$$\nabla_2\cdot(\rho_1^{\mathrm{i}}\boldsymbol{v}_0^{\mathrm{i}}+\rho_0^{\mathrm{i}}\boldsymbol{v}_1^{\mathrm{i}})=0, \tag{4.14a}$$

$$\rho_1^{\mathrm{i}}(\boldsymbol{v}_0^{\mathrm{i}}\cdot\nabla_2)\,\boldsymbol{v}_0^{\mathrm{i}}+\rho_0^{\mathrm{i}}(\boldsymbol{v}_1^{\mathrm{i}}\cdot\nabla_2)\,\boldsymbol{v}_0^{\mathrm{i}}+\rho_0^{\mathrm{i}}(\boldsymbol{v}_0^{\mathrm{i}}\cdot\nabla_2)\,\boldsymbol{v}_1^{\mathrm{i}}-\frac{1}{r}\rho_0^{\mathrm{i}}(v_{0,\theta}^{\mathrm{i}})^2\,\boldsymbol{i}_r+\nabla_2 p_1^{\mathrm{i}}$$
$$=-2\boldsymbol{\Omega}\times\boldsymbol{v}_0^{\mathrm{i}}-\boldsymbol{\Omega}\times(\boldsymbol{\Omega}\times\boldsymbol{r}). \tag{4.14b}$$

The r-component of (4.14*b*) relates $v_{1,r}^{\mathrm{i}}$ to the zeroth-order quantities. In the x- and θ-components of (4.14*b*), however, $v_{1,r}^{\mathrm{i}}$ does not occur, and we are left again with a two-dimensional problem. (Note that the right-hand side of (4.14*b*) has an r-component only.) The zeroth-order expansion of (4.14) yields

$$\boldsymbol{U}\cdot\nabla_2\rho_{10}^{\mathrm{i}}+\nabla_2\cdot\boldsymbol{v}_{10}^{\mathrm{i}}=0,\quad(\boldsymbol{U}\cdot\nabla_2)\,\boldsymbol{v}_{10}^{\mathrm{i}}+\nabla_2 p_{10}^{\mathrm{i}}=0, \tag{4.15a, b}$$

which results in $\rho_{10}^{\mathrm{i}}=p_{10}^{\mathrm{i}}=0$, $\boldsymbol{v}_{10}^{\mathrm{i}}=0$, in agreement with (2.9) and (3.13).

At 'infinity' the first-order velocity is thus given by $\boldsymbol{v}_{11}^{\mathrm{i}}=\boldsymbol{v}_{11}^{\mathrm{o}}$, where an expression for the latter quantity has been derived in the previous section, and similarly for the density and pressure. This implies that $\boldsymbol{v}_1^{\mathrm{i}}$, ρ_1^{i} and p_1^{i} are the first-order corrections (in ϵ) for the two-dimensional flow about a blade section, with the boundary conditions at infinity given by $\boldsymbol{v}=\boldsymbol{U}+\epsilon\boldsymbol{v}_{11}^{\mathrm{o}}$, $\rho=1+\epsilon\rho_{11}^{\mathrm{o}}$ and $p=1/\gamma+\epsilon p_{11}^{\mathrm{o}}$.

5. The second-order outer solution

At second order, the outer problem is given by

$$\nabla\cdot\boldsymbol{v}_2^{\mathrm{o}}+\boldsymbol{U}\cdot\nabla\rho_2^{\mathrm{o}}=-\frac{1}{r}\sum_{j=0}^{B-1}\boldsymbol{P}_j\cdot\nabla\delta(x)\,\delta\left(\theta-\frac{2\pi j}{B}\right), \tag{5.1a}$$

$$(\boldsymbol{U}\cdot\nabla)\,\boldsymbol{v}_2^{\mathrm{o}}+\nabla p_2^{\mathrm{o}}=-\boldsymbol{\Omega}\times\boldsymbol{v}_2^{\mathrm{o}}-\frac{1}{r}\sum_{j=0}^{B-1}[\boldsymbol{L}_{j,2}-\boldsymbol{D}_{j,2}\cdot\nabla]\,\delta(x)\,\delta\left(\theta-\frac{2\pi j}{B}\right), \tag{5.1b}$$

where in (5.1*a*) we have applied (3.8) and neglected the nonlinear terms. We now repeat the procedure of §3, i.e. we apply the operators $\boldsymbol{U}\cdot$ and $\nabla\cdot$ to (5.1*a*) and (5.1*b*) respectively, and find after subtraction

$$[(\boldsymbol{U}\cdot\nabla)^2-\nabla^2]\,p_2^{\mathrm{o}}=\sum_{j=0}^{B-1}\nabla\cdot\frac{1}{r}[\boldsymbol{L}_{j,2}-\boldsymbol{D}'_{j,2}\cdot\nabla]\,\delta(x)\,\delta\left(\theta-\frac{2\pi j}{B}\right), \tag{5.2}$$

with $\boldsymbol{D}' = \boldsymbol{D} + \boldsymbol{U}\boldsymbol{P}_j$ and where on the right-hand side the differential operators also apply to the δ-functions.

Next we write

$$p_2^0 = p_D + p_L, \tag{5.3}$$

where p_D is generated by the tensor $\boldsymbol{D}'_{j,2}$ and p_L by the vector $\boldsymbol{L}_{j,2}$. It will be shown next that the pressure corresponding to the right-hand side of (4.13) can be matched to p_D. Note that in the inner product of ∇ with $\boldsymbol{D}'_{j,2}$, from both left and right, the r-components do not contribute: see the remark on the r-component of $\boldsymbol{D}_{j,2}$ in §3. The procedure to determine the first term of the inner expansion of p_D, with respect to the blade at $\theta = 0$, is essentially the same as the one used to derive the expression for p_{10}^0. The result is

$$p_{D,0} = \frac{-1}{2\pi\beta_1} \frac{(D'_{0,2,ss} - \beta_1^2 D'_{0,2,qq})(\bar{s}^2 - \bar{q}^2) + \beta_1 (D'_{0,2,sq} + D'_{0,2,qs}) 2\bar{s}\bar{q}}{\bar{s}^2 + \bar{q}^2}. \tag{5.4}$$

The pressure which corresponds to the right-hand side of (4.13) is

$$-\frac{U}{2\pi} \frac{1}{(s^2+q^2)^2} [N_{2,s}(s^2 - q^2) + N_{2,q} 2sq)]. \tag{5.5}$$

Matching thus results in

$$D_{0,2,ss} - U^2 A/\epsilon^2 - \beta_1^2 D_{0,2,qq} = U\beta_1 N_{2,s}, \quad D_{0,2,sq} + D_{0,2,qs} = U N_{2,q}. \tag{5.6}$$

From Appendix B we have

$$N_{2,s} = \frac{-1}{\beta_1} \frac{UA}{\epsilon^2}, \quad N_{2,q} = \frac{-M_{p,2}}{U}, \tag{5.7}$$

We now find from (3.9), (3.10), (5.6) and (5.7)

$$D_{j,2,ss} = 0, \quad D_{j,2,sq} = -M_{p,2}, \quad D_{j,2,qs} = 0, \quad D_{j,2,qq} = 0. \tag{5.8}$$

The (second-order) pitching moment about the origin is given by

$$M_{p,2} = \tfrac{1}{2} U^2 \left(\frac{c}{\epsilon}\right)^2 \frac{1}{\beta_1} \left[2\mu_0 + \frac{\pi}{2}\alpha_0 - 2\pi \frac{d}{c}(\alpha - \alpha_0)\right], \tag{5.9}$$

where μ_0 is another constant determined by the camber line, and d is the position of the quarter-chord point relative to the origin, i.e. the intersection of the pitch change axis with the blade section, with the positive direction towards the trailing edge. Note that the pitching moment is a scalar, being the same for all blades at corresponding sections, and we therefore omit the subscript denoting the blade number.

In view of the discussion at the end of §4, the second-order circulation Γ_2 should be taken such that $\epsilon\Gamma_1 + \epsilon^2\Gamma_2$ is the circulation about the blade section in a two-dimensional flow, which is at infinity given by $\boldsymbol{v} = \boldsymbol{U} + \epsilon \boldsymbol{v}_{11}^0$, $\rho = 1 + \epsilon\rho_{11}^0$ and $p = 1/\gamma + \epsilon p_{11}^0$. It is therefore given by

$$\Gamma_2 = -U \frac{c}{\epsilon} \frac{\pi}{\beta_1} \left(\frac{v_{11,s}^0}{U\beta_1^2} \operatorname{sgn}(\Omega)(\alpha - \alpha_0) + \frac{v_{11,q}^0}{U} \right). \tag{5.10}$$

Now we can write down the outer pressure field up to second order. As we are mainly interested in this field because of its acoustic meaning, we will use an acoustically

more appropriate expression for the Green's function. By application of Fourier and Hankel transforms we find the following alternative to (3.16):

$$G(r,\theta,x\,|\,\rho,\phi,\xi) = \frac{1}{4\pi \mathrm{i}} \sum_{m=-\infty}^{\infty} \int_0^{\infty} \mathrm{e}^{\mathrm{i}m(\theta-\phi)} \frac{\gamma J_m(\gamma r)\, J_m(\gamma\rho)}{\kappa(\gamma, -m\Omega)} \times \exp\left(\frac{-\mathrm{i}}{\beta^2}[Mm\Omega + \operatorname{sgn}(x-\xi)\,\kappa(\gamma,-m\Omega)]\,(x-\xi)\right)\mathrm{d}\gamma, \quad (5.11)$$

where J_m is the Bessel function of the first kind and $\kappa^2(\gamma,\omega) = \omega^2 - (\gamma\beta)^2$, $\operatorname{Im}\kappa \leqslant 0$. If we use this to solve (3.15) and (5.2), we find

$$p_1^0 = \frac{-B}{4\pi \mathrm{i}} \sum_{n=-\infty}^{\infty} \int_0^{\infty} \int_{r_h}^{1} \mathrm{e}^{\mathrm{i}(nB\theta - k_x x)} \frac{\gamma J_{nB}(\gamma r)\, J_{nB}(\gamma\rho)}{\kappa(\gamma, -nB\Omega)} \left\{ L_{1,x}\,\mathrm{i}k_x - L_{1,\theta}\frac{\mathrm{i}nB}{\rho} \right\} \mathrm{d}\rho\,\mathrm{d}\gamma \quad (5.12)$$

and

$$p_2^0 = \frac{-B}{4\pi \mathrm{i}} \sum_{n=-\infty}^{\infty} \int_0^{\infty} \int_{r_h}^{1} \mathrm{e}^{\mathrm{i}(nB\theta - k_x x)} \frac{\gamma J_{nB}(\gamma r)\, J_{nB}(\gamma\rho)}{\kappa(\gamma, -nB\Omega)} \times \left\{ L_{2,x}\,\mathrm{i}k_x - L_{2,\theta}\frac{\mathrm{i}nB}{\rho} - D'_{2,xx}k_x^2 + (D'_{2,x\theta} + D'_{2,\theta x})\frac{nB}{\rho}k_x - D'_{2,\theta\theta}\left(\frac{nB}{\rho}\right)^2 \right\} \mathrm{d}\rho\,\mathrm{d}\gamma, \quad (5.13)$$

where k_x is the axial wavenumber:

$$k_x = [MnB\Omega + \operatorname{sgn}(x)\,\kappa(\gamma, -nB\Omega)]/\beta^2. \quad (5.14)$$

In deriving (5.12) and (5.13) we have used the fact that the components of $\boldsymbol{L}$ and $\boldsymbol{D}$, in a cylindrical coordinate frame, are the same for all blades, which enabled us to drop the subscript j and to sum over j. Furthermore, the r-component of $\boldsymbol{L}$ is negligible in the thin airfoil approximation. In the inertial coordinate frame, in which the propeller rotates but does not translate, the angular coordinate is given by $\tilde{\theta} = \theta + \Omega t$. In this coordinate frame the pressure is thus expressed as a sum of the harmonics of the blade passing frequency, which is the motivation for using (5.11), instead of (3.16).

In (5.12) and (5.13) the contributions to the noise from lift, thickness, and pitching moment are clearly distinguishable. Note that in the present hierarchy the thickness noise is of second order, i.e. of higher order than the loading noise. The expression for the latter can be regarded as an improved version of Gutin's result, which is only valid in the far field (Gutin 1948).

If (5.12) is used in (3.27) we find for the first-order outer velocity field

$$\begin{aligned} \boldsymbol{v}_1^0 = \frac{\mathrm{i}B}{4\pi M} \sum_{n=-\infty}^{\infty} \boldsymbol{\nabla} \int_0^{\infty} \int_{r_h}^{1} \gamma J_{nB}(\gamma r)\, J_{nB}(\gamma\rho) \\ \times \left\{ \frac{1}{\kappa} \frac{\beta^2}{\dfrac{nB\Omega}{M} + \operatorname{sgn}(x)\,\kappa} \mathrm{e}^{\mathrm{i}(nB\theta - k_x x)} \left[k_x L_{1,x} - \frac{nB}{\rho} L_{1,\theta} \right] \right. \\ \left. + H(x) \frac{2}{\gamma^2 + \left(\dfrac{nB\Omega}{M}\right)^2} \mathrm{e}^{\mathrm{i}nB(\theta + \Omega x/M)} \frac{nB}{\rho M} U L_{1,q} \right\} \mathrm{d}\rho\,\mathrm{d}\gamma \\ - H(x) \frac{1}{r} \frac{U}{M} \sum_{j=0}^{B-1} \boldsymbol{L}_1 \delta\left(\frac{\Omega}{M} x + \theta - \frac{2\pi j}{B} \right). \end{aligned} \quad (5.15)$$

The contribution of the first term between curly brackets is the (first-order) acoustic particle velocity, the contribution of the second term is the convective velocity associated with the downstream wake. In the latter term the integration over γ can be performed analytically, which yields

$$\frac{iB}{2\pi M}\sum_{n=-\infty}^{\infty}\nabla H(x)\,e^{inB(\theta+\Omega x/M)}\int_{r_h}^{1} I_{nB}\left(r_< \left|\frac{nB\Omega}{M}\right|\right)K_{nB}\left(r_> \left|\frac{nB\Omega}{M}\right|\right)\frac{nB}{\rho M}UL_{1,q}\,d\rho, \tag{5.16}$$

where $r_< = \rho$, $r_> = r$ for $\rho < r$ and $r_< = r$, $r_> = \rho$ for $\rho > r$. The above expression is equivalent to one found by Hanson (1991, §7) for the wake-associated part of the downwash angle. Hanson also shows that the last term in (5.15) is cancelled by singularities in (5.16). This was shown previously by Lordi & Homicz (1981) for the case of a ducted rotor.

6. The numerical application of the present method

In this section we first apply the theory, as presented so far, to a $\frac{1}{5}$ scale model of the six-bladed Fokker 50 propeller, which has been used for aerodynamic measurements in the NLR Low Speed Wind Tunnel (Kooi & De Wolf 1988) and for acoustic measurements in the German–Dutch Windtunnel (DNW) (Schulten 1988). The value of the perturbation parameter ϵ, according to (2.1), for this propeller is 0.15. The operating conditions of the case we will consider were $M = 0.12$ and $\Omega = -0.67$.

The central part of the numerical application of the present method is the calculation of the downwash velocity v_{11}^0 from (3.37), (3.26) and (3.39). In order to evaluate the Cauchy principal value in (3.37), we use the following relation, which can be derived from (3.38):

$$\mathrm{P}\int_{r_h}^{1}[I(\rho)-I_{as}(\rho)]_{s=0,\,q=0}\,d\rho = \mathrm{P}\int_{r_h}^{1}\left[I(\rho)-\frac{\Gamma_1(\rho)}{\Gamma_1(r)}I_{as}(\rho)\right.$$
$$\left.+(\rho-r)\frac{I_{as}(\rho)}{\Gamma_1(r)}\frac{d\Gamma_1(\rho)}{d\rho}\right]_{s=0,\,q=0}d\rho+\frac{M}{4\pi U}\Gamma_1(r)\frac{1-r_h}{(r-r_h)(1-r)}, \tag{6.1}$$

which is expressed in the scalar variable Γ_1 by use of (4.10), to shorten the notation. Note that the last term cancels the second term on the right-hand side of (3.37). Next we make use of the following approximations involving Tchebycheff polynomials:

$$\left[I(\rho)-\frac{\Gamma_1(\rho)}{\Gamma_1(r)}I_{as}(\rho)\right]_{s=0,\,q=0}\approx\frac{\sin\chi}{\cos\chi-\cos\chi_r}\sum_{n=0}^{N}a_n\cos(n\chi), \tag{6.2a}$$

$$\left[(\rho-r)\frac{I_{as}(\rho)}{\Gamma_1(r)}\frac{d\Gamma_1(\rho)}{d\rho}\right]_{s=0,\,q=0}=\frac{M}{4\pi U}\frac{1}{\rho-r}\frac{d\Gamma_1(\rho)}{d\rho}$$
$$\approx\frac{-M}{4\pi U}\left(\frac{2}{1-r_h}\right)^2\frac{1}{\sin\chi}\frac{1}{\cos\chi-\cos\chi_r}\frac{d}{d\chi}\sin\chi\sum_{n=0}^{N}b_n\cos(n\chi), \tag{6.2b}$$

where $\chi(\rho)=\cos^{-1}(2(\rho-r_h)/(1-r_h)-1)$ and $\chi_r=\chi(r)$. We have assumed here that the lift behaves as $(\rho-r_h)^{\frac{1}{2}}$ at the hub and as $(1-\rho)^{\frac{1}{2}}$ at the tip; with respect to the behaviour at the hub this assumption is incorrect, but, as already mentioned in §2, the hub region contributes little to the aerodynamics and acoustics of a propeller.

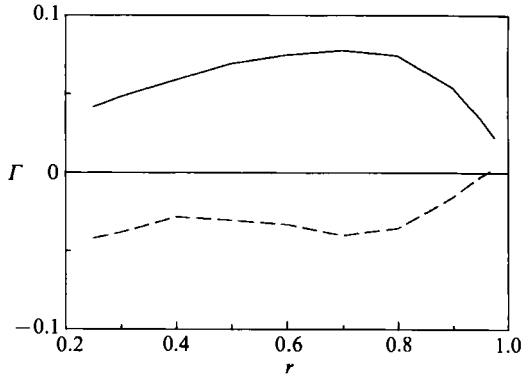

FIGURE 3. The first- (——) and second-order (– – – –) approximations for the circulation.

The coefficients a_n and b_n can be determined such that the right-hand sides of (6.2a, b) are least-squares approximations of the left-hand sides, evaluated at a given set of radii $\{r_i\}$. The relation between the coefficients a_n and b_n and the set $\{\Gamma_1(r_i)\}$ is linear, e.g. a matrix $\boldsymbol{B}$ can be found such that

$$b_n = \sum_i B_{ni} \frac{\Gamma_1(r_i)}{\sin(\chi_i)}, \tag{6.3}$$

see, for example, Dahlquist & Björck (1974, p. 92). The integration of the right-hand sides of (6.2a, b) can be done analytically by using (Glauert 1959, p. 92):

$$\mathrm{P}\int_0^\pi \frac{\cos n\chi}{\cos\chi - \cos\chi_r}\,\mathrm{d}\chi = \pi \frac{\sin|n|\chi_r}{\sin\chi_r}. \tag{6.4}$$

We thus find for the first term at the right-hand side of (6.1):

$$[v^0_{11,\theta}]_{j=0} = \frac{1-r_\mathrm{h}}{2}\pi\left[-\cos\chi_r a_0 - \tfrac{1}{2}\cos 2\chi_r a_1 + \sum_{n=2}^{N} \sin n\chi_r \sin\chi_r a_n\right]$$
$$-\frac{2}{1-r_\mathrm{h}}\frac{M}{4U}\left[b_0 + \frac{1}{\sin\chi_r}\sum_{n=1}^{N}(n\sin\chi_r\cos n\chi_r + \sin n\chi_r\cos\chi_r)\,b_n\right]. \tag{6.5}$$

Note that an expansion like the right-hand side of (6.2a), and hence the application of (6.4), is not possible for the integrand at the left-hand side of (6.1), owing to its non-vanishing values at the integration boundaries. The other parts of v^0_{11} can be calculated with standard numerical integration methods.

In figure 3 the first- and second-order approximations of the circulation, i.e. $\epsilon\Gamma_1$ and $\epsilon\Gamma_1 + \epsilon^2\Gamma_2$, are plotted as a function of the radius. It is quite clear from this plot that our supposition that the second term is of order ϵ with respect to the first term, is not satisfied. In fact, the sum is negative over the whole blade, corresponding to a negative thrust, which is unphysical for the present conditions. We thus have to conclude that, although the circulation (and other quantities) can formally be expanded in powers of ϵ, the coefficients of this expansion are too large for it to be of use when ϵ is equal to 0.15 (or comparable values).

Like any asymptotic series, the expansion for the circulation is divergent and the

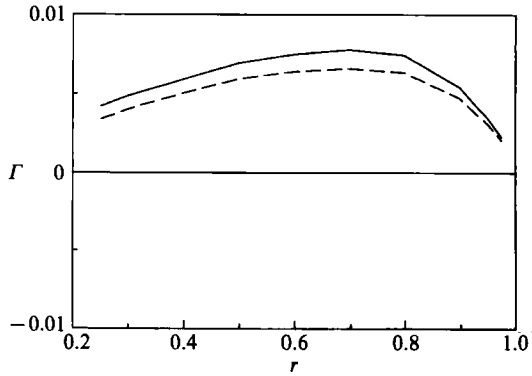

FIGURE 4. The first- (——) and second-order (– – – –) approximations for the circulation, chord divided by 10.

most accurate result is found by breaking off the expansion after a definite (usually small) number of terms; for the present case this number appears to be equal to one, and adding more terms will only worsen the result.

To illustrate the role of the magnitude of ϵ, we have plotted in figure 4 $\epsilon\Gamma_1$ and $\epsilon\Gamma_1+\epsilon^2\Gamma_2$ for the same case, with the chord of each blade section divided by 10, resulting in $\epsilon = 0.015$. Although such a propeller is not very realistic, this calculation shows that for this ϵ the asymptotic theory yields plausible results.

It will be shown in the next section how the present calculation method can be modified in order to be useful for larger perturbation parameters as well. This modified method will also be used to obtain a better understanding of the problem encountered in this section.

7. The modified calculation method

In this section we will show how the analytical expressions we have derived for the downwash velocity v_{11}^0, can still be of use, despite the disappointing results of the previous section. Suppose that we write the relation between the first and second term of the asymptotic expansion for the circulation as

$$\Gamma_2 = \mathrm{L}\Gamma_1, \tag{7.1}$$

where L is a linear operator (see (5.10)), involving an integration in radial direction. Instead of calculating Γ_2 by application of (7.1), we now solve the following equation:

$$\Gamma = \epsilon(\Gamma_1+\mathrm{L}\Gamma), \tag{7.2}$$

which, in the case of $\Omega = 0$, is equivalent to Prandtl's integral equation for lifting wings, see (3.41). Note that if the method of matched asymptotic expansions were strictly applicable, i.e. if $\epsilon\Gamma_2 \ll \Gamma_1$, (7.1) and (7.2) would yield the same results (see also Van Holten 1976; Van Dyke 1975, p. 172). However, even in the case of helicopter blades, which have a very high aspect ratio, difficulties are met when (7.1) is applied (Johnson 1986). However, the analogue of (7.2) has been applied in a quite favourable validation of Van Holten's theory (Pierce & Vaidyanathan 1981).

Note that the fact that the second-order circulation is not small compared to the first-order circulation does not mean that the downwash angle α_{dw} is large (i.e. of order unity); it just means that α_{dw} is not small compared to $\alpha-\alpha_0$. In fact, the

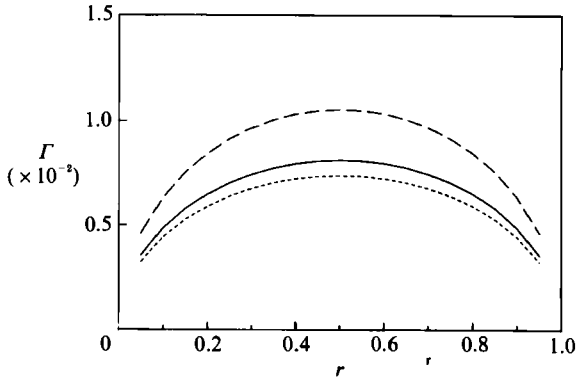

FIGURE 5. The circulation about an elliptic wing, $A = 6.67$: ——, integral equation; — —, first order; – – – –, second order.

induced velocity is small compared to the zeroth-order velocity U, i.e. of order ϵ, which enables us to keep using the linear operator L.

In order to solve (7.2) we could use an iterative procedure, the first step of which is the application of (7.1). As this procedure is not always convergent however, we solve (7.2) for a given set of radii $\{r_i\}$ by matrix inversion, which involves the use of matrix $\boldsymbol{B}$ of (6.3). To illustrate the meaning of (7.2) we first apply it to the same example as Van Dyke, i.e. a flat elliptic wing ($\Omega = 0$, $B = 1$), and we choose the aspect ratio to be $A = 6.67$, i.e. $\epsilon = 0.15$.

In figure 5 the first- and second-order approximations of the asymptotic theory (i.e. $\epsilon\Gamma_1$ and $\epsilon\Gamma_1 + \epsilon^2\Gamma_2$) as well as the solution of the integral equation (7.2) (i.e. Γ) are plotted. It is easily checked that these results agree with the analytical results for an elliptic wing:

$$\epsilon\Gamma_1 + \epsilon^2\Gamma_2 = (1-2\epsilon)\,\epsilon\Gamma_1, \quad \Gamma = \frac{\epsilon\Gamma_1}{1+2\epsilon}. \tag{7.3a, b}$$

Furthermore, we notice that the asymptotic approximation yields much better results for the stationary wing than it did for the propeller. The two most important differences between a wing and a propeller, i.e. a propeller rotates and has at least two blades, appear to enhance the three-dimensional effects. This is not difficult to understand, considering the fact that the wake of a wing consists (at first order) of a single flat sheet, whereas the wake of a propeller consists of a multiple helix, which means that the flow at each blade section is considerably influenced by the other sections of both the same blade and the other blades. This causes the coefficient in front of the second term of the asymptotic expansion for the circulation, which equals 2 in (7.3a), to be significantly larger in the case of a propeller than a wing. In other words, the 'effective' aspect ratio of a propeller blade is smaller than the aspect ratio of a wing of comparable span and chord. As the distance between a blade section and the nearest wake of another blade is proportional to B^{-1}, it might be better to take ϵB as the small parameter, which is close to 1 for the present example.

To investigate the influence of the number of blades and angular velocity a little further, we have calculated the circulation for the same propeller as in the previous section, for four cases: $B = 6$ and 2, combined with both $\Omega = -0.67$ and 0. In the case of $\Omega = 0$ we have 'untwisted' the blade to such an extent that the geometrical angle of incidence at each section is the same for all cases. The results are plotted in figure 6(a–d), which shows clearly that both the reduction of the number of blades and

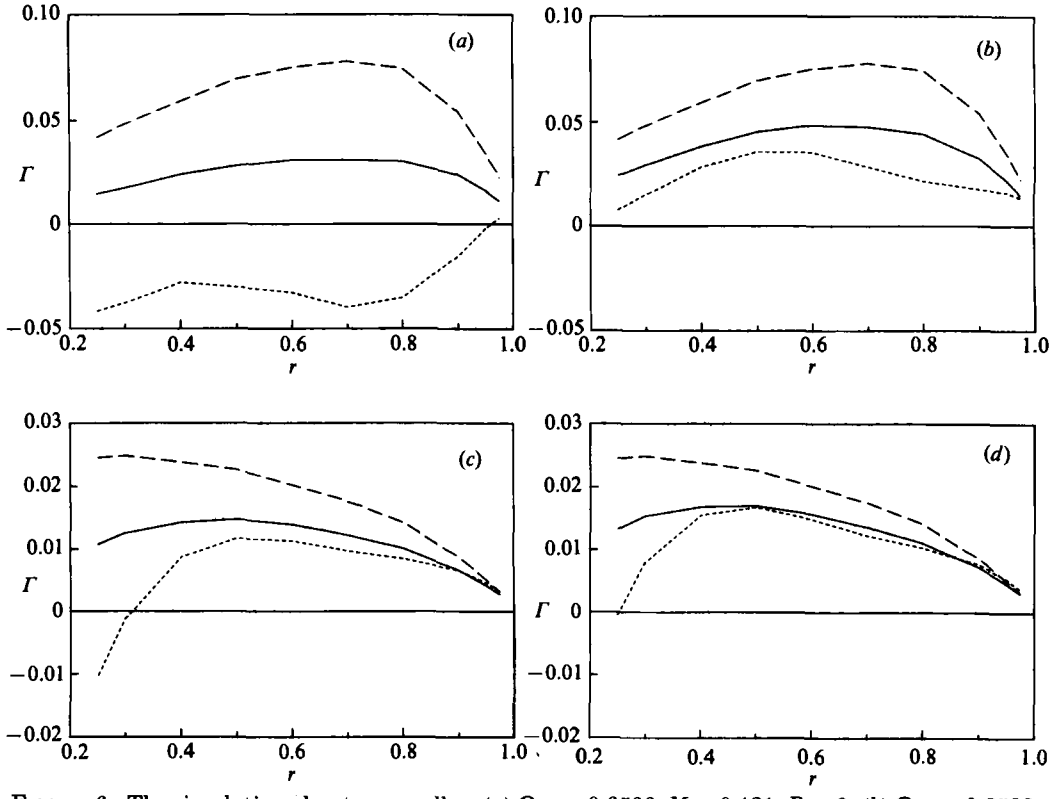

FIGURE 6. The circulation about a propeller: (*a*) $\Omega = -0.6566, M = 0.121, B = 6$; (*b*) $\Omega = -0.6566$, $M = 0.121$, $B = 2$; (*c*) $\Omega = 0$, $M = 0.121$, $B = 6$; (*d*) $\Omega = 0$, $M = 0.121$, $B = 2$. ——, Integral equation; ——, first order; – – –, second order.

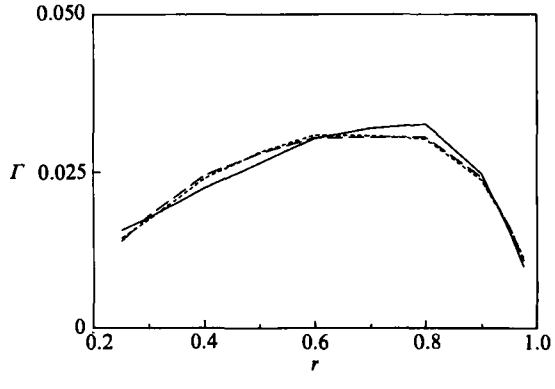

FIGURE 7. The solution of (7.2) for $N = 2$ (——), 3 (——), and 4 (– – –).

taking $\Omega = 0$ significantly improve the results of the asymptotic theory. For $\Omega = 0$ the curves deviate from each other near the hub, which is a consequence of the choice of the basis functions in (6.2); these functions are not suitable for a stationary wing with the planform of a propeller blade.

In order to investigate the influence of the number of basis functions used in (6.2), we have plotted the results for Γ for $N = 2$, 3, and 4 in figure 7. It turns out that, at least for the present case, $N = 3$ yields sufficient accuracy.

It should be reiterated that (7.2), which is applicable for larger values of ϵ than (7.1), is not the result of a consistent asymptotic expansion. As pointed out by Van Dyke, the third term in the asymptotic expansion for, for example, the circulation about an elliptic wing, the first two terms of which are given by the right-hand side of (7.3*a*), is logarithmic in ϵ. This term cannot be extracted from (7.3*b*). In the next section we will compare some results obtained by the application of (7.2) to experimental results, which will give us an indication of the usefulness of the present (modified) method for the prediction of propeller aerodynamics and acoustics.

8. Comparison to experimental data

The thrust and power coefficients of the $\frac{1}{5}$ scale model of the six-bladed Fokker 50 propeller have been measured in the NLR Low Speed Wing Tunnel at various free-stream velocities, advance ratios, and blade settings (Kooi & De Wolf 1988). For the present comparison we have selected the measurements at a free-stream velocity of 40 m/s and a blade angle (at 0.7 radius) of 28°. The computations were carried out on a 386/25 MHz personal computer, equipped with a math coprocessor, on which each calculation (for one advance ratio) took about 5 min.

In figures 8 and 9 the thrust and power coefficients are plotted as a function of the advance ratio. The discrepancies between the present results and the experimental data are some 5% on the average, with a maximum of 9% at the lowest advance ratio.

In §6 it was mentioned that the basis functions chosen to describe the spanwise distribution of the circulation do not behave correctly at the hub. In order to check the consequence of this we compare the calculated spanwise load distribution, i.e. $\mathrm{d}C_t/\mathrm{d}r$, with the experimental values from Kooi & De Wolf for $J = 0.589$, see figure 10. The latter data were obtained from wake velocity measurements and are corrected for the contraction. The agreement is very good and there are no indications that the actual behaviour at both the hub and the tip is not captured by the present method.

For $J = 0.57$ another method, based on strip-theory combined with a two-dimensional viscous inner method, has been applied as well. The results, indicated by crosses, are some 11% higher than the experimental data. The latter method generated the pressure distributions used by Schulten (1988) for his acoustic calculations. These calculations consisted of solving the linearized Euler equations with full incorporation of the boundary conditions, i.e. the source term of the convected wave equation was determined by the detailed blade geometry and the pressure distribution on the blades, which amounts to an application of the Ffowcs Williams–Hawkings equation without the quadrupole term (Ffowcs Williams & Hawkings 1969).

Next we will compare the acoustic results of the present theory to Schulten's results and the experimental data. The acoustic pressure is given by (see (5.12) and (5.13))

$$p_{\mathrm{ac}} = \frac{-B}{4\pi} \sum_{n=-\infty}^{\infty} \int_0^{\infty} \int_{r_h}^{1} \mathrm{e}^{\mathrm{i}(nB\theta - k_x x)} \frac{\gamma J_{nB}(\gamma r)\, J_{nB}(\gamma\rho)}{\kappa(\gamma, -nB\Omega)}$$

$$\times \left\{ L_x k_x - L_\theta \frac{nB}{\rho} + \mathrm{i}\epsilon^2 \left[D'_{2,xx} k_x^2 - (D'_{2,x\theta} + D'_{2,\theta x}) \frac{nB}{\rho} k_x + D'_{2,\theta\theta} \left(\frac{nB}{\rho} \right)^2 \right] \right\} \mathrm{d}\rho\, \mathrm{d}\gamma, \quad (8.1)$$

where $\boldsymbol{L}$ is the lift which is determined by the solution of (7.2). Some numerical

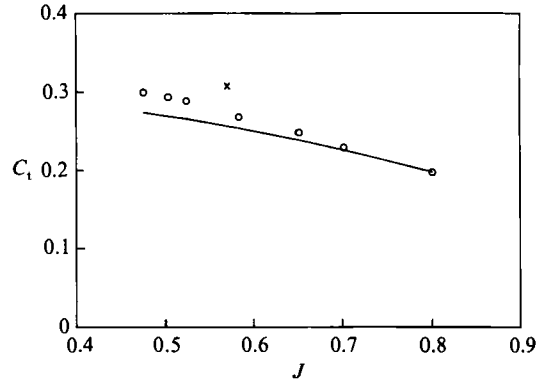

FIGURE 8. The thrust coefficient as a function of the advance ratio: ——, present results; ○, experiments; ×, strip theory.

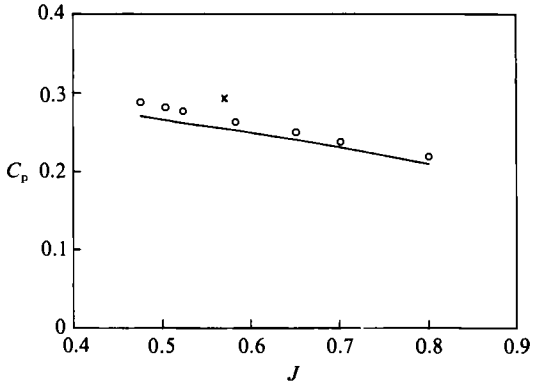

FIGURE 9. The power coefficient as a function of the advance ratio. Notation as figure 8.

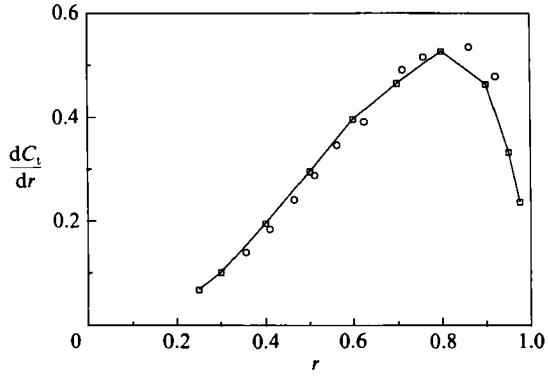

FIGURE 10. Spanwise load distribution for $J = 0.589$: —□—, theory; ○, experiment.

aspects of the integral in (8.1) as well as a far-field approximation can be found in Brouwer (1989).

It can be shown that the loading and thickness noise parts of (8.1) equal the corresponding expressions derived by Hanson (1985) if: (i) the chordwise distributions occurring in Hanson's work are replaced by δ-functions; and (ii) the downwash angle α_{dw} is neglected in the present work. These differences illustrate that

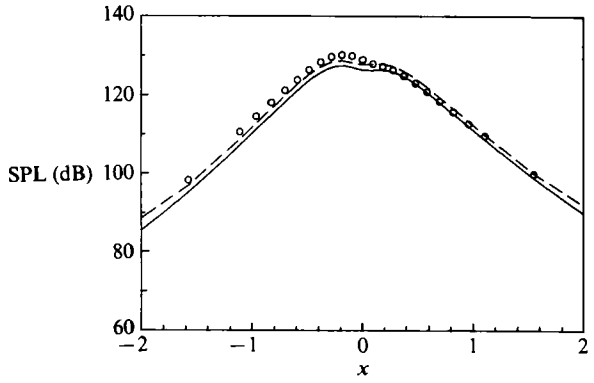

FIGURE 11. Sound pressure level, BPF, $r = 1.32$: ——, present results; — —, Schulten (1988); ○, experiments.

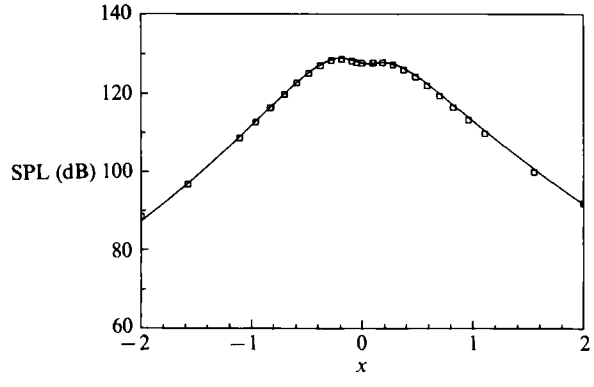

FIGURE 12. Comparison to Schulten's results (□), same aerodynamic input: ——, present results.

Hanson's lifting surface theory is more suitable for propfans which have very thin blades (of low aspect ratio) and are thus designed for small angles of attack (and consequently small downwash angles).

The computing time for each case, comprising the calculation of the sound pressure of one harmonic at 50 points in the x-direction for a constant value of r, was again about 5 min. In figure 11 the absolute value of the first harmonic (i.e. the BPF tone) of p_{ac} is plotted as a function of x for $r = 1.32$. The comparison of this result with the experimental results shows a reasonable agreement. The results obtained by Schulten show a somewhat better agreement with the experimental values. A closer inspection shows that the differences between the two sets of theoretical results can be ascribed entirely to the differences in the aerodynamic input. In figure 12 we have plotted the results of both aeroacoustic computations with the same aerodynamic data as input, i.e. the data used by Schulten. It is obvious that both aeroacoustic methods give virtually the same answer, at least for the blade passing frequency of this propeller.

The phase angle of the first harmonic of p_{ac} is plotted in figure 13, together with the experimental values and Schulten's results. The (almost constant) difference between both the theoretical results and the experimental results has not been explained yet.

This section is concluded with the results at $r = 3.9$, shown in figures 14 and 15. In

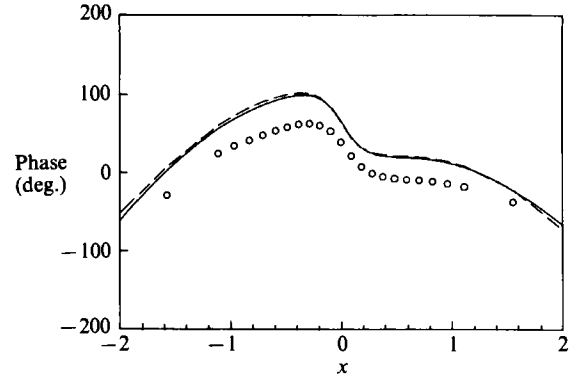

FIGURE 13. Phase angle, BPF, $r = 1.32$. Notation as figure 11.

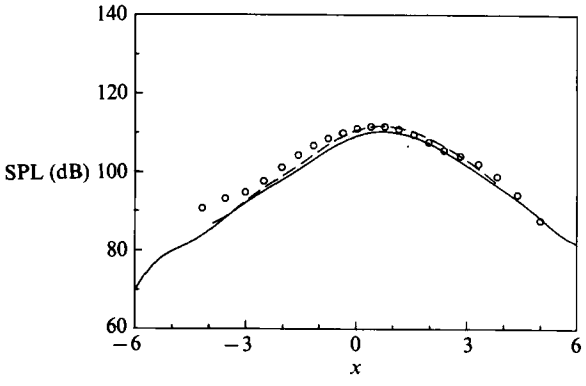

FIGURE 14. Sound pressure level, BPF, $r = 3.9$. Notation as figure 11.

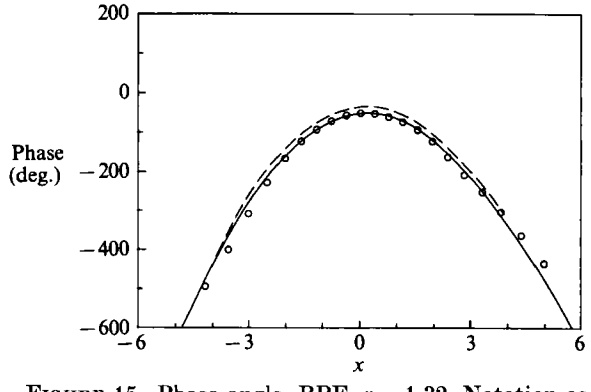

FIGURE 15. Phase angle, BPF, $r = 1.32$. Notation as figure 11.

this case the agreement with both the measured sound pressure level and the measured phase angle is good.

9. Conclusions

Van Dyke's method of matched asymptotic expansions has been applied to the case of a propeller with blades of high aspect ratio in an axial uniform flow. In combination with thin airfoil theory, the method yields an asymptotic series for the

circulation about a propeller blade, the first two terms of which are explicitly derived in this paper; the first term is the value found after application of two-dimensional airfoil theory to each blade section, the second term is a correction caused by the three-dimensional character of the problem. When applied to a typical case, however, the results turned out to be unphysical, which is because the expansion parameter of the problem, i.e. the reciprocal of the aspect ratio of a blade, is not small enough for realistic propellers. It appears that, in comparison to stationary wings, three-dimensional effects are more important, which leads to a smaller 'effective' aspect ratio.

This problem was remedied by transforming the approximation of the circulation by two terms into an integral equation. A numerical solution to this equation yielded, for the cases considered, results for the thrust and power coefficient which agree well with the experimental values. Once the circulation is known, the acoustic pressure can be calculated. The present formulation incorporates both loading and thickness noise. Comparison to the results of Schulten's theory, in which details of the pressure distribution in the chordwise direction are taken into account, shows an almost exact agreement, while the agreement with experimental values is reasonable.

The present method clearly shows that the aerodynamic and acoustic theories for propellers are closely related; the objective of both theories is the calculation of the flow perturbation. Indeed, the methods pertaining only to the acoustics of a propeller require the output data, for example pressure distributions, of an aerodynamic method.

Besides giving some insight into the fundamentals of propeller theory, the present method also provides the basis for a practical calculation method, which yields both performance and noise data, with a minimum of computational effort.

The author thanks J. B. H. M. Schulten for the many helpful discussions.

Appendix A

In this Appendix we discuss the multipole expansion of the source term in the momentum equation, (3.6). The derivation of (3.7) and (3.8) from (3.5) proceeds along the same lines. Consider a section of the propeller blade at $\theta = 0$, of infinitesimal width, extending from r to $r + \mathrm{d}r$, as depicted in figure 16. Let us assume that we may write the following multipole expansion:

$$p' \nabla S \, \delta(S) = \frac{1}{r} [- \boldsymbol{L}(r) + \boldsymbol{D}(r) \cdot \nabla + \ldots] \, \delta(x) \, \delta(\theta), \tag{A 1}$$

where $S = 0$ determines the surface of the blade as explained in the main text, and $\boldsymbol{D}$ is a tensor of rank two. Below, we will consider only the first two terms at the right-hand side.

We integrate (A 1) over a volume V_s, which is bounded by $r = r_s$ and $r = r_s + \mathrm{d}r$ and such values of θ and x that V_s contains the blade section under consideration and no parts of the other blades. We then find for the left-hand side:

$$\int_{V_s} p' \nabla S \, \delta(S) \, \mathrm{d}^3 r = \mathrm{d}r \int_{C(r_s)} p' \boldsymbol{n} \, \mathrm{d}l, \tag{A 2}$$

where $C(r_s)$ is the boundary contour of the section at $r = r_s$, $\mathrm{d}l$ is the differential arclength, and $\boldsymbol{n}$ is the normal vector of length unity on the blade surface. The

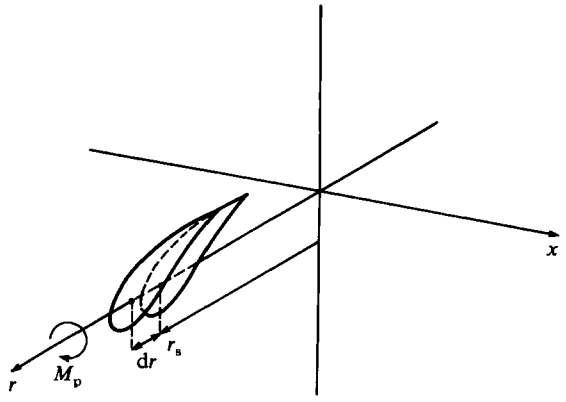

FIGURE 16. Blade section of width dr.

integral over the second term on the right-hand side of (A 1) is zero, and the integral over the first term is trivial. We thus find

$$\boldsymbol{L}(r_s) = -\int_{C(r_s)} p'\boldsymbol{n}\,\mathrm{d}l, \tag{A 3}$$

i.e. $\boldsymbol{L}(r)$ is the lift per unit length on the blade section at r. Note that its direction is not necessarily perpendicular to the pitch change axis.

Next we take the inner product of (A 1) with the vector $\boldsymbol{r}-\boldsymbol{r}_s$, where $\boldsymbol{r}_s$ is given by $(r_s, 0, 0)$, and subsequently integrate over V_s. For the left-hand side we find

$$\int_{V_s} (\boldsymbol{r}-\boldsymbol{r}_s)\cdot[p'\nabla S\,\delta(S)]\,\mathrm{d}^3r \approx \mathrm{d}r\int_{C(r_s)} p'(\boldsymbol{r}-\boldsymbol{r}_s)\cdot\boldsymbol{n}\,\mathrm{d}l. \tag{A 4}$$

The integral over the first term on the right-hand side of (A 1) is proportional to $(\mathrm{d}r)^2$ and gives zero contribution in the limit $\mathrm{d}r\to 0$. The second term can be integrated by parts, and we then find

$$D_{xx}(r_s)+D_{\theta\theta}(r_s) = -\int_{C(r_s)} p'(\boldsymbol{r}-\boldsymbol{r}_s)\cdot\boldsymbol{n}\,\mathrm{d}l. \tag{A 5}$$

Finally we consider the r-component of the cross product of $\boldsymbol{r}-\boldsymbol{r}_s$ with (A 1), which gives

$$D_{x\theta}(r_s)-D_{\theta x}(r_s) = \int_{C(r_s)} p'[(\boldsymbol{r}-\boldsymbol{r}_s)\times\boldsymbol{n}]_r\,\mathrm{d}l. \tag{A 6}$$

The right-hand side is equal to the negative of the pitching moment (M_p) on the blade section, with its positive direction depicted in figure 16. Summation of (A 1) over all the blades yields (3.6).

Appendix B

First, consider a blade section in an incompressible two-dimensional flow. The coordinate frame to be used in this Appendix is depicted in figure 17. Note that the notation is independent of the notation in the main text. The velocity potential at large distances is approximated by

$$\phi = Ux+\frac{\Gamma}{2\pi}\chi-\frac{\boldsymbol{N}\cdot\boldsymbol{r}}{2\pi r^2}. \tag{B 1}$$

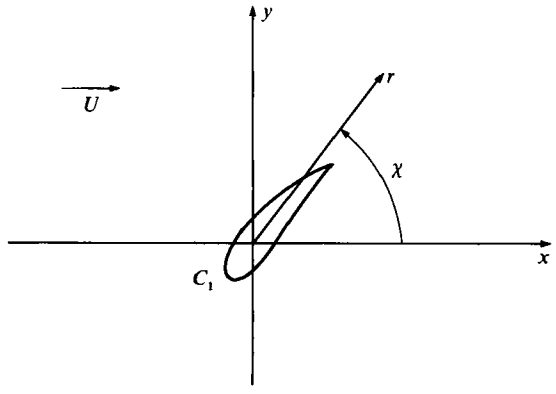

FIGURE 17. The coordinate system used in Appendix B.

The (dimensionless) momentum equation reads

$$(\boldsymbol{v}\cdot\boldsymbol{\nabla})\,\boldsymbol{v}+\boldsymbol{\nabla}p=0. \tag{B 2}$$

Let C_1 denote the contour defined by the blade section boundary, and let C_2 be a circular contour of radius R at a large distance. The area enclosed by C_1 and C_2 is denoted by S. Now we take the inner product of (B 2) with $\boldsymbol{r}$ and integrate over S:

$$\int_S \boldsymbol{r}\cdot[(\boldsymbol{v}\cdot\boldsymbol{\nabla})\,\boldsymbol{v}+\boldsymbol{\nabla}p]\,\mathrm{d}^2r$$

$$=\int_{C_1+C_2}(\boldsymbol{r}\cdot\boldsymbol{v}\,\boldsymbol{n}\cdot\boldsymbol{v}+p\boldsymbol{n}\cdot\boldsymbol{r})\,\mathrm{d}l-\int_S(\boldsymbol{r}\cdot\boldsymbol{v}\,\boldsymbol{\nabla}\cdot\boldsymbol{v}+v^2+2p)\,\mathrm{d}^2r \tag{B 3a}$$

$$=\int_{C_1}p\boldsymbol{n}\cdot\boldsymbol{r}\,\mathrm{d}l+\int_{C_2}(\boldsymbol{r}\cdot\boldsymbol{v}\,\boldsymbol{n}\cdot\boldsymbol{v}+[p_\infty+\tfrac{1}{2}(U^2-v^2)]\,\boldsymbol{n}\cdot\boldsymbol{r})\,\mathrm{d}l-(2p_\infty+U^2)\,(\pi R^2-A) \tag{B 3b}$$

$$=0, \tag{B 3c}$$

where A is the area of the blade section. In the last step Bernoulli's theorem has been used. The second term of (B 3b) can be calculated from (B 1), which yields

$$N_x=-\frac{1}{U}\left[\int_{C_1}(p-p_\infty)\,\boldsymbol{n}\cdot\boldsymbol{r}\,\mathrm{d}l+U^2A-\frac{\Gamma^2}{4\pi}\right]. \tag{B 4}$$

The same procedure can be used for the z-component of the cross-product of r with (B 2). The result is

$$N_y=-M_p/U. \tag{B 5}$$

This result can also be found in Milne-Thomson (1958, p. 92), where it is derived from Blasius' theorem.

To find the corresponding expressions in a compressible flow, within the thin airfoil approximation, we may apply the Prandtl–Glauert transformation, and neglect the nonlinear terms:

$$N_x=-\frac{1}{\beta}UA, \tag{B 6}$$

whereas the expression for N_y is unchanged.

REFERENCES

BROUWER, H. H. 1989 A lifting line model for propeller noise. *AIAA Paper* 89-1079.

CRIGHTON, D. G. & LEPPINGTON, F. G. 1973 Singular perturbation methods in acoustics: diffraction by a plate of finite thickness. *Proc. R. Soc. Lond.* A **335**, 313–339.

DAHLQUIST, G. & BJÖRCK, A. 1974 *Numerical Methods*. Prentice-Hall.

FFOWCS WILLIAMS, J. E. & HAWKINGS, D. L. 1969 Sound generation by turbulence and surfaces in arbitrary motion. *Phil. Trans. R. Soc. Lond.* A **264**, 321–342.

GLAUERT, H. 1959 *The Elements of Aerofoil and Airscrew Theory*, 2nd Edn (reprinted). Cambridge University Press.

GOLDSTEIN, S. 1929 On the vortex theory of screw propellers. *Proc. R. Soc. Lond.* A **123**, 440–465.

GUTIN, L. 1948 On the sound field of a rotating propeller. *NACA TM* 1195.

HANSON, D. B. 1985 Near-field frequency-domain theory for propeller noise. *AIAA J.* **13**, 449–504.

HANSON, D. B. 1986 Propeller noise caused by blade tip radial forces. *AIAA Paper* 86-1892.

HANSON, D. B. 1991 Unified aeroacoustics analysis for high speed turboprop aerodynamics and noise, Volume I – Development of theory for blade loading, wakes, and noise, *NASA CR* 4329.

HANSON, D. B. & FINK, M. R. 1979 The importance of quadrupole sources in prediction of transonic tip speed propeller noise. *J. Sound Vib.* **62**, 19–38.

JOHNSON, W. 1986 Recent developments in rotary-wing aerodynamic theory. *AIAA J.* **24**, 1219–1244.

KOOI, J. W. & DE WOLF, W. B. 1988 Aerodynamic measurements on a 1/5 scale model of the Fokker 50 propeller and comparison with theoretical predictions. In *Advanced Propellers & Their Installation on Aircraft*. Cranfield Institute of Technology, UK.

LIEPMANN, H. W. & PUCKETT, A. E. 1947 *Introduction to Aerodynamics of a Compressible Fluid*. John Wiley.

LORDI, J. A. & HOMICZ, G. F. 1981 Linearized analysis of the three-dimensional compressible flow through a rotating annular blade row. *J. Fluid Mech.* **103**, 413–442.

MILNE-THOMSON, L. M. 1958 *Theoretical Aeordynamics*. Dover.

PIERCE, G. A. & VAIDYANATHAN, A. R. 1981 Helicopter rotor loads using a matched asymptotic expansions technique. *NASA CR* 165748.

PRANDTL, L. & TIETJENS, O. G. 1957 *Applied Hydro- and Aerodynamics*. Dover.

REISSNER, H. 1937 On the vortex theory of the screw propeller. *J. Aero. Sci.* **5**, 1–7.

SCHULTEN, J. B. H. M. 1984 Aerodynamics of wide-chord propellers in non-axisymmetric flow. *AGARD Symp. on Aerodynamics and Acoustics of Propellers*, Toronto, *Paper* 7.

SCHULTEN, J. B. H. M. 1988 Frequency-domain method for the computation of propeller acoustics. *AIAA J.* **26**, 1027–1035.

SPARENBERG, J. A. 1984 *Elements of Hydrodynamic Propulsion*. Martinus Nijhoff.

VAN DYKE, M. D. 1964 Lifting-line theory as a singular perturbation problem. *Appl. Maths Mech.* **28**, 90–102.

VAN DYKE, M. D. 1975 *Perturbation Methods in Fluid Mechanics*. Stanford: The Parabolic Press.

VAN HOLTEN, TH. 1975 The computation of aerodynamic loads on helicopter blades in forward flight, using the method of the acceleration potential. Thesis, Delft University of Technology.

VAN HOLTEN, TH. 1976 Some notes on unsteady lifting line theory. *J. Fluid Mech.* **77**, 561–579.

VAVRA, M. H. 1960 *Aero-thermodynamics and Flow in Turbomachines*. John Wiley.

WILMOTT, P. 1988 Unsteady lifting-line theory by the method of matched asymptotic expansions. *J. Fluid Mech.* **186**, 303–320.